Ab Initio Structure of the Active Site of Phosphotriesterase

M. Krauss†

Center Advanced Research Biotechnology/NIST, Rockville, Maryland 20850

Received June 5, 2000

This research exploits two recent developments to obtain a fundamental understanding of the metalloenzyme active site using the bimetallic enzyme phosphotriesterase as an example of this class. First is the theoretical prediction that the structure and spectroscopy of a native metalloenzyme active site is qualitatively determined by the supermolecule complex of the metal(s) and the first shell of ligands with proper charge states including waters directly bonded to ionic ligands. The second is the development of an effective potential for representing the molecular environment interacting with an all-electron active site in the quantum Hamiltonian. The GAMESS suite of electronic structure codes has implemented this new methodology, effective fragment potentials (EFP), to make theoretical calculations on structure, spectroscopy, and reactivity tractable for systems involving hundreds of atoms. Since there are transition metal cations at the active site of these enzymes, the all-electron part of the complex is calculated with relativistic compact effective potentials (CEP) and their concomitant basis sets. A realistic representation of the active site with its protein environment can be obtained using a combination of the CEP and EFP. This presentation will determine the inherent electronic and structural characteristics of phosphotriesterase using ab initio quantum mechanical methods. A single X-ray structure for the Zn−Zn enzyme is leveraged to obtain the structure of the Cd−Cd enzyme and to examine the consequences of protonating the active site.

1. INTRODUCTION

An understanding of the geometric and electronic structure of the active site of a metalloenzyme can now be obtained theoretically. The size of the active site requires a methodology that realistically partitions the system into an all-electron region and interactive environment. This is now possible using the effective core potential (EFP) method[1,2] to decompose the quantum Hamiltonian and the effective core potentials (ECP)[3,4] to reduce the calculation of the all-electron system to manageable size. This study will focus on the organophosphorus hydrolase from *Pseudomonas diminuta*, phosphotriesterase (PTE), which catalyzes the hydrolysis of paraoxon, sarin, soman, and other inhibitors of acetylcholinesterase.[5,6] This enzyme has been extensively studied with much emphasis on the effect on reactivity with metal substitution[7] and mutations.[8] X-ray structures, of the bimetallic Zn−Zn[9] and Cd−Cd[10] enzymes, provide the basis for studying the detailed binding and mechanism. However, the available experimental structures are insufficient to deduce a complete view of binding and reactivity in PTE or even the ionicity of the active site.

This study will leverage the available experimental structural information for the calculation of the electronic and structural geometry of the active site. Metalloenzyme active sites are very ionic, and the local binding energy of the first-shell complex exceeds the interaction energies of the protein environment with the active site. Early work suggested that the inherent structure of the metal active site is perturbed weakly by the protein environment.[11] Metal−ligand distances and angles in a large data set of zinc proteins are found to agree well with ideal values deduced from small zinc complexes.[12−14] Recent accurate work on copper enzymes illustrates this in detail for the native structures and, furthermore, shows that accurate spectral properties can be obtained from these inherent complexes.[15−18] The inherent structure of the complex is defined here as the in vacuo theoretically optimized or minimally constrained structure, with the ligands arranged to be topologically compatible with a given experimental structure. However, Ryde has demonstrated that even weak perturbations can have apparently large effects on the conformation because the energy surface can be very flat for different conformations of the ligands.[19] We have observed similar behavior for both bimetallic enzymes, zinc lactamase and phosphotriesterase.[20] The protein environment around the active site in the native enzyme can then accommodate the active site first-shell complex with little strain but will affect the protonation state of the ligands and thus the ionicity of the site. Preliminary studies of the PTE active site[20,21] and zinc lactamase[22,23] have neglected the explicit protein environment but have supported the contention that the inherent and experimental structures are similar. In this study the effect of the protein environment on the structure will be explored for the zinc and cadmium enzymes of PTE. The bare active site only will be explored for two ionicities. In one the bridging ligand is chosen to be a hydroxyl anion, and in the second the site is protonated at the bridging ligand or one of the ligands.

The first step in the theoretical protocol is the calculation of the inherent structure of the first-shell active site of the enzyme. A single experimental structure can be leveraged with theoretical calculations to study the effect of metal substitution, mutations, or a variety of substrates on the structure. This is particularly important in PTE where the activity varies widely with metal and mutations are of interest to engineer specificity and activity. The protein environment for the enzymes with different metals is found to be

† E-mail: krauss@carb.nist.gov. Telephone: (301) 738-6242.

10.1021/ci000046b
Published on Web 09/13/2000

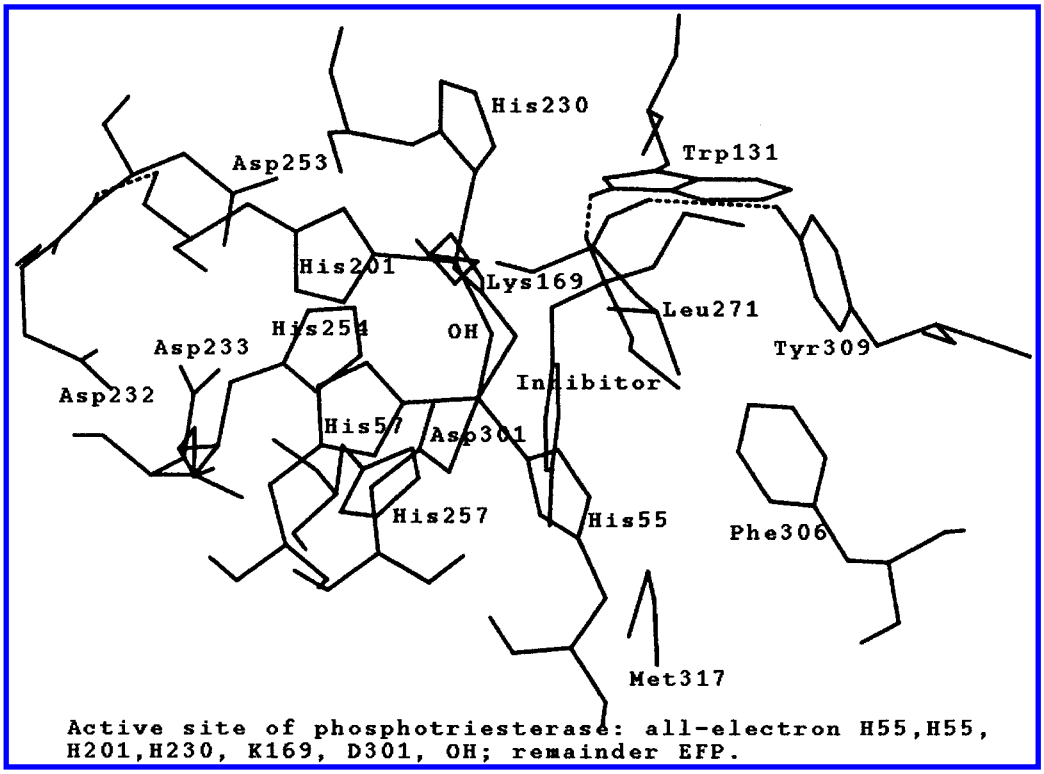

Figure 1. Schematic of active site of phosphotriesterase.

essentially the same in the X-ray structures, and in vacuo optimized structures have been compared favorably for the bimetallic enzyme PTE.[20] This study compared the X-ray structures for the Zn−Zn[9] and Cd−Cd[10] enzymes and predicted the structure for the Cd−Zn enzyme. The in vacuo theoretical structure for the Zn−Zn enzyme differs mostly from the X-ray in the orientation of the histidines, H55, H201, and H230, which interact with the bound inhibitor or are hydrogen bonded to an interior residue. The inhibitor did not bind to the Cd−Cd enzyme, and a calculation of the structure of this enzyme that started from the theoretical Zn−Zn structure yields a Cd−Cd structure we consider to be in good agreement with the X-ray.[20] Gradient optimized Hartree−Fock and density functional structures are in good agreement, suggesting that electron correlation effects are not important for closed-shell divalent transition metal cation complexes. However, there is a basis set effect with the Zn−Zn distance of 3.46 Å obtained with the double-ζ (DZ) basis about 0.2 Å larger than the value obtained with the DZd basis.

PTE is a bimetallic enzyme. The two metals are bound with two bridging ligands, a hydroxyl and a carbamylated lysine. As seen in the schematic Figure 1, Zn1 is also bound to two histidines and an aspartate while Zn2 is bound only to two histidines. Cd1 has the same coordination as Zn1 while at least one additional water is bound to Cd2 in the X-ray structure. An inhibitor is bound in the structure found for the zinc enzyme but not for the cadmium enzyme. This will affect the observed water coordination and, perhaps, the orientation of the ligands. The Asp301 is hydrogen bonded to the bridging hydroxyl, which is a structural motif that is found often in bimetallic enzymes.[24] The second shell of residues around the active site toward the interior or protein will strongly affect the behavior with respect to ligand binding and mutations. The residues toward the protein (the interior) are involved in hydrogen bonds with the first shell of residues (see Figure 1). Hydrogen bonds to Od2(D301) and Nϵ(H201) could be important in maintaining conformation and ionicity in the first shell of the active site. All the residues toward solution (the exterior) are hydrophobic, and one residue, Trp181, is quite close to Zn2 and its associated histidines. It has been noted that these residues provide a hydrophobic box into which the substrate must fit and also limit the number of waters near the metal site. Examination of the X-ray structure shows that the phosphonate inhibitor also has a hydrogen bond to the Trp181. The role of the hydrophobic residues on the solvent side of the active site is shown by the experimental structure to restrict the orientation of the substrate as well as access of water.

The role of the bridging ligands in the mechanism is not directly obvious from the structure. The suggestion has been made that water could act as a bridging ligand[21] in the Zn−Zn structure. There is also considerable confusion on the ionicity of the bridging ligand for the Cd structure. The reported distances[10] of the bridging oxygen to the Cd^{2+} are too large for the ligand to be a hydroxyl anion. However, more than one water will be present and refinement of the charge density in this region is noted by the experimentalists to be difficult. In this paper we will analyze the conformations of the first-shell active site in the presence of the local protein environment. This paper is primarily designed to show the capabilities of a combined ECP/EFP calculation. Analysis of substrate binding, the hydrolysis reaction, and the effect of first-shell mutants on active site conformation have also been studied but go beyond the limited goals of this paper and will be presented elsewhere.

2. METHODS

Calculating binding and reaction paths at enzyme active sites has recently been made tractable by the use of the

effective fragment potential (EFP) method.[1,2] The enzyme active site is divided into two regions, the chemically active region and the protein environment. The chemically active region, substrate and relevant protein residues, is treated by ab initio all-electron quantum chemistry, while the environment or spectator region is described by EFP that represent the electrostatic, polarization, charge transfer, and repulsive interactions for the complex in the Hamiltonian. With the use of the EFP, ab initio quantum chemical calculations are tractable for an active site that consists of hundreds of atoms. The EFP integrals and gradients have been implemented in GAMESS,[25] allowing optimization of substrates within the active site and the determination of transition states. The current implementation of the EFP method includes Coulombic, polarization (classical induction), and nonbonded exchange repulsion.[4] In the present implementation, the Coulombic and polarization terms are calculated directly within GAMESS. The repulsive terms are obtained by fitting the interactions of the all-electron terms for the expected orientations with the hydrogen-bonded interactions for the hydrophilic residues and the overlap repulsions for the hydrophobic ones.[26] The repulsive EFP were parametrized with the assumption that a water molecule can simulate the range of interactions.

A model of the active site (quantum motif) can be obtained from a relevant X-ray structure or extracted from a molecular dynamics simulation. In this case all the calculations start from the X-ray structure of the Zn−Zn enzyme. The backbone atoms of the Zn and Cd enzymes superimpose within 0.2 Å,[9,10] and all metal substituted PTE enzymes can start from any structure. The calculation of the inherent structure of the first-shell active site of the Cd−Cd enzyme has already been initiated from the Zn enzyme.[20] The first-shell active site was shown to be in reasonable agreement with experiment for a hydroxyl bridging ligand except for the disagreement with the distances to the bridging oxygen and some ligand orientations.

In this paper the active sites will be optimized for Zn−Zn and Cd−Cd with a hydroxyl anion bridge and with either the hydroxyl bridging ligand or the Asp carboxylate protonated. A full first shell of EFP will be included. Preliminary analysis of the structures obtained by addition of the proton without the full shell of EFP will also be discussed. Other choices are possible for placing the added proton and will be examined later, but this range of systems describes the capabilities of the ECP/EFP methodology and is most relevant to the comparison with the X-ray structure. In this procedure the X-ray structure for the Cd−Cd enzyme is used only for comparison with the calculations and not to initiate any calculation.

Comparable first-shell active sites are considered here. No additional water is bound to the first shell beyond the bridging ligand. Water binding is intimately tied to the binding of substrates and will be examined in that context for both the Zn and Cd enzymes. Binding of water should not qualitatively affect the conformation of the first-shell active site for PTE although it can for other metalloenzymes, but the orientations of ligands can be affected by the neglect of the waters. The first-shell active site is defined as described in Figure 1 to consist of the two metal cations and the following ligands: D301, H55, H57, H230, H201, K169 with the lysine carbamylated. All the residues are considered all-electron with all atoms included back to the C_α atom. In one case, H230, the amide backbone, was also included since there are backbone hydrogen-bonded interactions to the interior protein. For both the Zn−Zn and Cd−Cd enzymes with the hydroxyl ligand, two calculations were performed. One froze the coordinates of all the C_α carbons, and the other allowed all these atoms to be unconstrained. All the imidazole ligands (histidines) were maintained neutral. The protein environment is represented by EFP with all the neighboring residues fixed at the positions found in the Zn enzyme for all calculations. If all the atoms represented in the EFP calculation were represented by all-electron basis functions, there would be a total of 1244 basis functions rather than the 538 needed for the calculation with the hydroxyl anion. The residues represented by EFP are W131, D232, D233, H254, D253, H257, L271, M317, F306, and Y309.

All optimizations were done at the Hartree−Fock level using the CEP 4-31G basis set concomitant to the effective core potentials.[3,4] Comparison of the PTE structures optimized with HF or DFT methods showed little difference.[20] A selected set of structure optimizations is presented here to illustrate the application of the ECP and EFP. The Zn−Zn active site is optimized with the C_α both constrained and unconstrained, while the Cd−Cd active site is presented for just the unconstrained optimization. An 'inherent' structure for the protonated Zn−Zn and Cd−Cd active sites is presented as well as the unconstrained optimization with the EFP for the protonated Cd−Cd enzyme. The default condition for optimization in GAMESS was not achieved since the number of iterations exceeded 300 and required a large amount of computer time. Nevertheless, all runs were below a maximum root-mean-square deviation (rmsd) of 0.0009 bohr/hartree. The Zn−Zn enzyme with frozen coordinates optimized to a rmsd of 0.0003 bohr/hartree. The large number of degrees of freedom is an essential difficulty compounded by the strong coupling between high and low-frequency modes leading to a rather soft effective potential around the metal cations. In the preliminary optimizations that neglected the EFP protein field, optimizations were more complete and all reached values of rmsd of 0.0001.

3. RESULTS AND DISCUSSION: ACTIVE SITE STRUCTURES

The Zn−Zn active site was optimized both with the C_α constrained and unconstrained in the presence of an EFP to represent the interactions with the first shell of residues surrounding the active site. The final structure of the constrained optimization is shown in Figure 2. Both the all-electron active site (Figure 2a) and the site with the EFP (Figure 2b) are presented for clarity. The most significant bond distances in the site for both optimizations are compared in Table 1 with the experimental values. All distances are then in agreement within the experimental accuracy for the bond lengths of about 0.2 Å with the exception of the O(D301) and O(K169) distances to Zn1. However, the accuracy of the oxygen positions is in doubt since the geometry of the Schiff base N−H bond and the carboxylate distances were previously shown to be inconsistent with the electronic structure of these moieties in the active site.[20] For example, the N−C bond distance is calculated to be 1.35 Å,

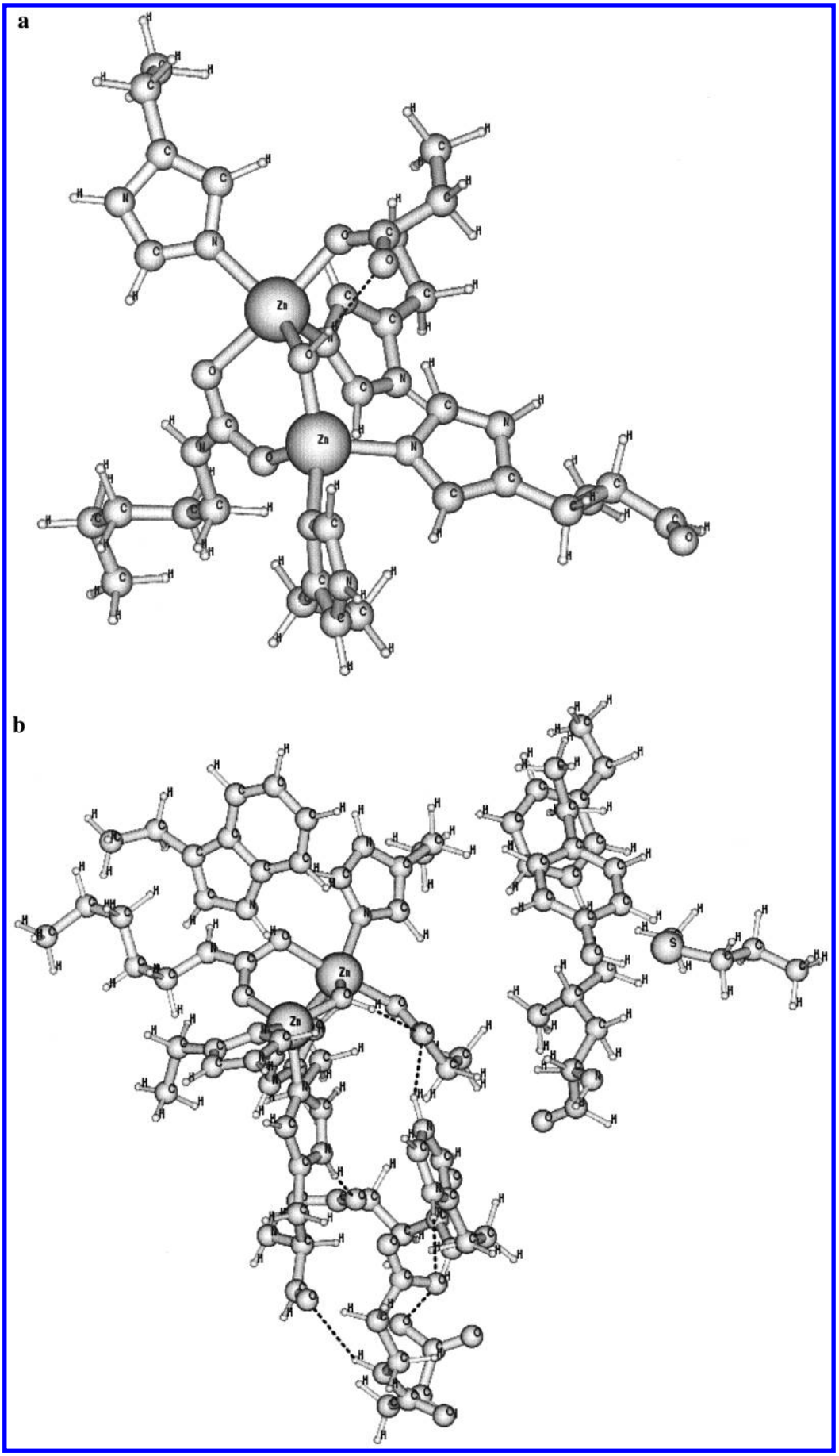

Figure 2. (a) Optimized active site for Zn−Zn PTE: all-electron atoms. (b) Optimized active site for Zn−Zn PTE: all-electron and EFP atoms.

Table 1. Comparison between X-ray and Computed Bond Distances (Å) in Zn−Zn and Cd−Cd Active Site

	Zn X-ray	constrain	unconstrain	Cd X-ray	unconstrain	add H^+
M−N(H57)	1.91	2.21	2.08	2.15	2.30	2.26
M−N(H55)	1.84	2.07	2.08	2.04	2.34	2.25
M−N(H201)	2.15	2.11	2.01	2.44	2.32	2.28
M−N(H230)	2.01	2.01	2.09	2.09	2.24	2.20
M−O(D301)	2.38	2.06	2.11	2.48	2.29	2.46
M−O(K169)	2.38, 1.81	2.14, 1.97	2.21, 1.98	2.41, 2.30	2.33, 2.20	2.24, 2.17
M−OH	1.93, 1.93	2.01, 1.92	2.00, 1.94	2.62, 2.68	2.21, 2.15	2.35, 2.28
M−M	3.31	3.37	3.48	3.79	3.78	

Table 2. Comparison of a Dihedral Angle (Cda−Cdb−N1−C2) Orienting the Histidine Ligands for the Cd−Cd Enzymes

residue	X-ray	in vacuo	Cd−Cd(0)	Cd−Cd(+1)
H55	−156	61	−175	−165
H57	−55	−50	−41	−59
H201	−154	26	−61	−96
H230	11	38	10	20

consistent with a double bond, while the experimental value is 1.46 Å. The C−N single bond distance is chosen initially for the refinement. The fit to the charge density for a resolution exceeding 2 Å apparently does not detect the double bond. This discrepancy will affect all the distances in the binding of the carbamylated moiety with the zinc cations. As noted earlier,[20] the X-ray carboxylate bond distances are also not consistent with the expected electronic behavior of this side chain bound to the zinc divalent cation. The oxygen bound to the metal with the largest effective positive charge will have the shorter metal−O distance but the longer C−O distance. This is what is calculated but not found in the X-ray structure. The X-ray structure is not consistent with the expected electronic structure. The problem probably arises from the initial choice of coordinates that is not corrected in the refinement. The calculated Zn−Zn distance is 3.37 Å for the constrained and 3.48 Å for the unconstrained, and both can be considered in good agreement with the experimental value of 3.31 Å.

The total energy between the constrained and unconstrained conformations is large, of the order of 28 kcal/mol. The energy of deforming the backbone has to be comparable but is not included in this calculation. For the Zn−Zn enzyme, there is a substantial shift in the C_α for all residues but K169, H57, and D301. The EFP do not hold the entire residue in place through their interactions, just the side chains.

The Cd−Cd enzyme was optimized with frozen C_α and without constraints but with the same environment described by the EFP that was used for the Zn−Zn enzyme. The experimental X-ray structures find the protein backbone for both proteins are the same within experimental error. For the experimental resolution, a mean coordinate error of about 0.2 Å is expected. We expect metal substitution generally only affects the first shell but both side-chain orientations and the backbone may be affected. The calculation of the constrained and unconstrained active sites will provide insight into whether a single X-ray structure is sufficient to initiate the optimization for other metals. The bond distances in Table 1 shows the agreement is good between the unconstrained optimization (Figure 3a,b) and X-ray values except for the Cd distances to the bridging hydroxyl (water). The constrained optimization, however, does not agree even in the qualitative aspects of the residue orientations with the Cd−Cd metals as seen in Figure 3c where the D301 binds in bidentate fashion to the Cd and does not make a H-bond to the bridging hydroxyl. The constrained Cd−Cd distance is quite small at 3.54 Å. The larger metal distorts the first shell sufficiently that an unconstrained optimization is required. The EFP interactions from the frozen second shell produce accurate first-shell bond distances and angles, but they are not significantly different from the values reported earlier[20] for the unconstrained optimization of the bare active site. However, the orientations of the histidine ligands are improved with the inclusion of the EFP as seen by examining the dihedral angle from Cda−Cdb−N1−C2. The C2 atom is measured clockwise from the N1 attached to the metal. The dihedral angles for H55 and H201 disagree the most between the X-ray and in vacuo optimization of the first-shell active site as seen in Table 2, but the EFP values agree better with experiment for the "neutral" Cd−Cd and even better for the structure with the protonated asp301. The orientation of these ligands is affected by the H-bonds to the interior residues and also by the neglect of water ligands bound directly or through H-bonds to the metals.

The large values for the bridging oxygen distances to the Cd cannot result from the presence of the bridging water. A bridging hydroxyl anion is calculated to have a much shorter distance, and a water does not act as a bridging ligand as we show below. As we suggested in the earlier analysis based on the inherent structure, the presence of additional binding waters yields a X-ray density that is difficult to refine. There are at least two waters bound to the active site in addition to the bridging hydroxyl, and they may be found in multiple sites. A future study will examine the effect on the structure of water(s) bound directly to the bridging hydroxyl anion.

The H-bond network from the protein to the first-shell active site does yield some surprising bond distances and also provides the basis for the orientations observed for the residues in the experimental structure. The N−H bond in H230 is substantially extended to 1.06 Å by the H-bond to E253. The carboxylate from E253 also H-bonds to the N−H in H55 but more weakly since this oxygen is shared with a backbone amide. The N−H in H55 is extended but only to 1.01 Å. The H-bond from H254 to the carboxylate of D301 is important structurally by maintaining the orientation of the carboxylate side chain but also in modulating the local ionicity of the active site. In the in vacuo optimization there is a tendency for the OD2 atom in the D301 carboxylate to interact with the H(C) imidazole bond, but this weak interaction cannot compete with the stronger H-bonds in the EFP model.

The ionicity of the residues in the EFP was chosen to reflect the ionicity chosen initially for the active site. To stabilize the carboxylate/hydroxyl H-bond between two anions, H254 was chosen to have a protonated imidazole side chain which is itself bound to an anionic carboxylate from D233. The carboxylate in E253 is chosen to be an anion, but the substantial increase in the N−H bond in the

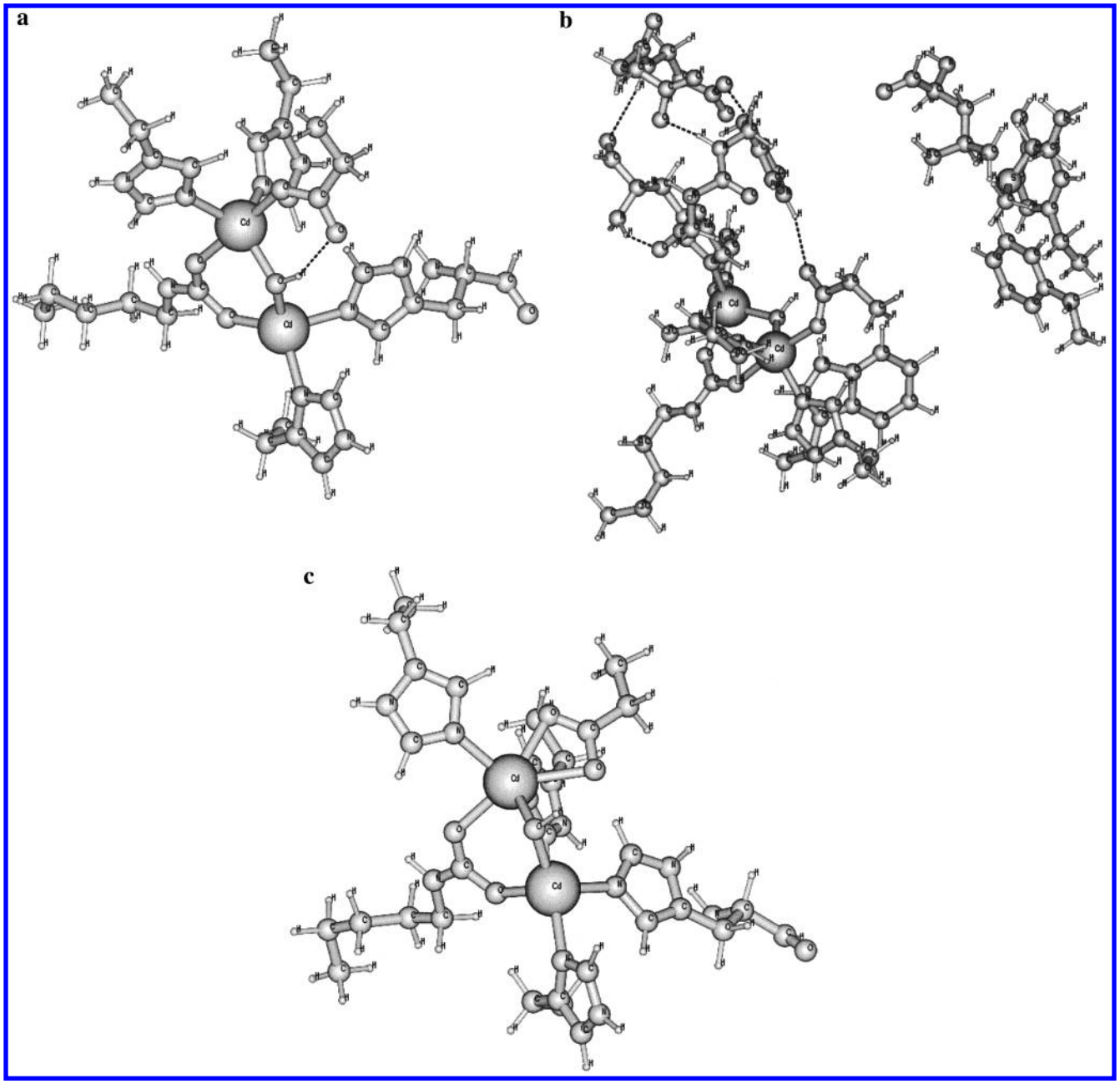

Figure 3. (a) Optimized active site for Cd−Cd PTE: all-electron atoms. (b) Optimized active site for Cd−Cd PTE: all-electron and EFP atoms. (c) Constrained optimization of Cd−Cd PTE active site: all-electron atoms.

H230 imidazole suggests that a transfer of the proton is a possible model. An anionic histidine could have substantial effects on the structure of the first shell. A number of different arrangements of the proton among the environment residues is possible and may be close energetically. Since no proton is transferred to solution, these rearrangements are not observed as p*K* inflections. However, they could also occur as part of a protonation event that involves movement of a proton in more than one group.

Several studies show that deprotonation of an active site functional group is required for activity.[27,28] Since these studies were prior to the structural characterization of the active site, the catalytically important histidines were identified as the functional group. Another possibility is the addition of a proton to the D301 carboxylate/hydroxyl H-bond complex.[21] The pK_a observed for the Zn−Zn enzyme is 5.8, but it is substantially higher at 8.1 for Cd−Cd. The Zn−Zn crystal was formed at a pH of 7.5 and Cd−Cd at a pH of 9.0,[9,10] suggesting that the ionicity is the same with a bridging hydroxyl anion for the different metal enzyme crystal structures. Two binding sites are explored here for the proton attached to the D301 carboxylate and to the bridging hydroxyl. The inherent structure of the protonated Zn enzyme determines the proton bound to the carboxylate of the D301 in the optimized structure. An initial structure with a bridging water transferred the proton to the carboxylate in the course of the optimization as seen in Figure 4a. For the Cd enzyme, the optimization was initiated again with a bridging water. Water was maintained in the course of the optimization, but the Cd−Cd distance became very large. The presence of another water had no effect on this behavior as seen in Figure 4b. When the distance exceeded 5 Å, the calculation was stopped before convergence. These inherent model calculations were done with the histidine side chain

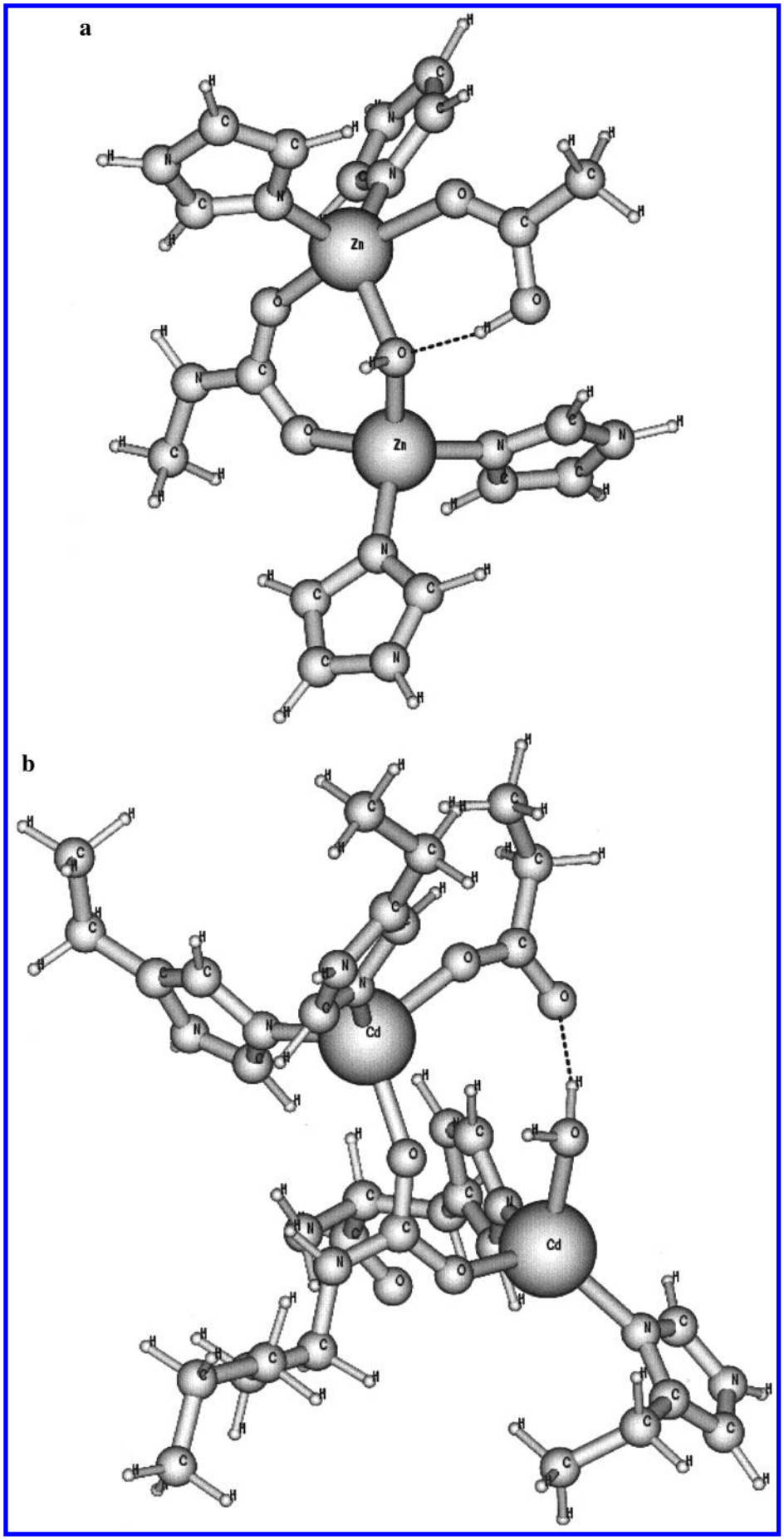

Figure 4. (a) Protonated Zn phosphotriesterase inherent structure, metal bonds to the bridging ligands are not disrupted, proton bound to carboxylate. (b) Protonated Cd−Cd phosphotriesterase inherent structure: Cd−Cd atoms separate with water ligand.

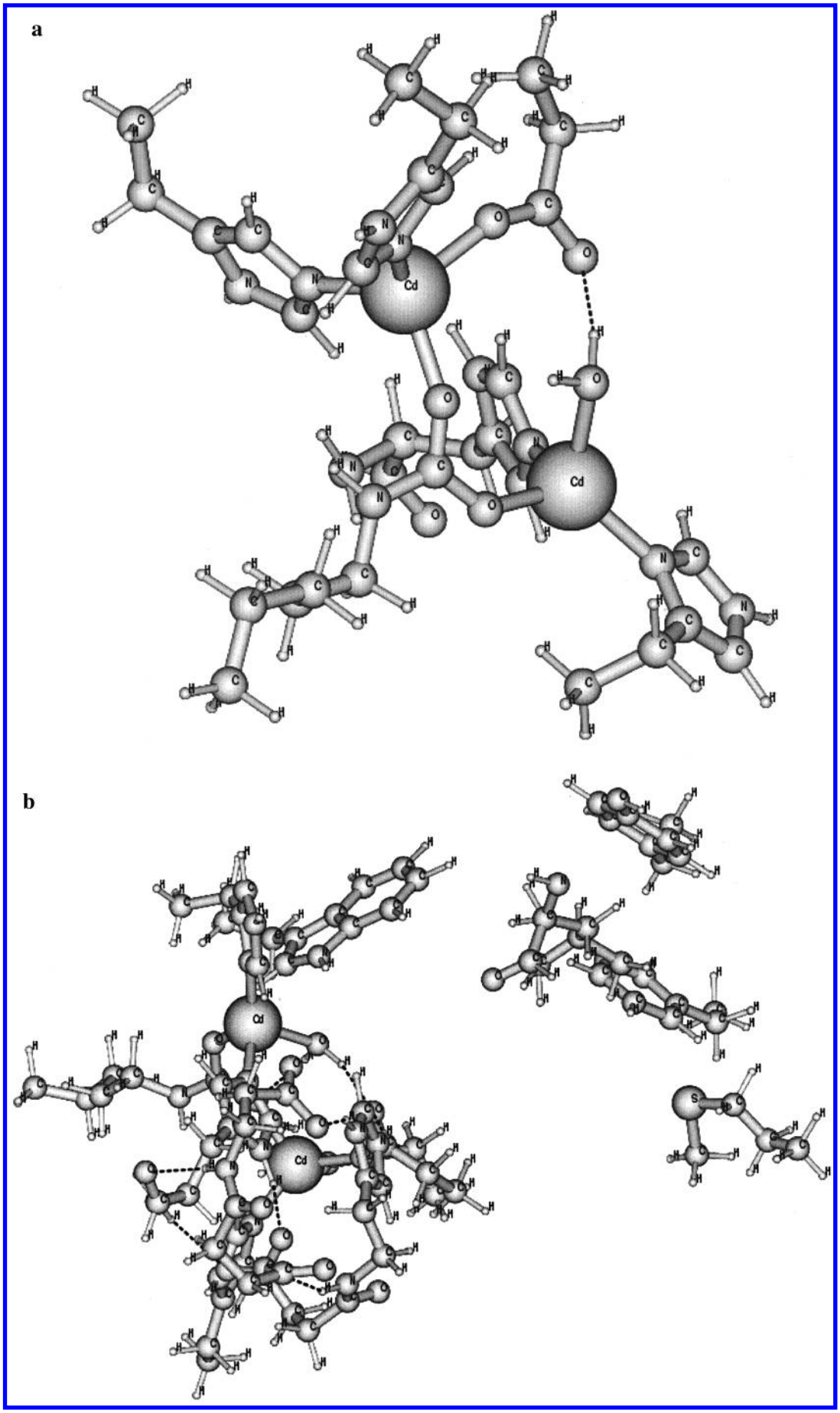

Figure 5. (a) Unconstrained structure of the protonated Cd−Cd active site: hydroxyl to water, all-electron atoms. (b) Unconstrained structure of the protonated Cd−Cd active site: hydroxyl to water, all-electron atoms, and EFP atoms.

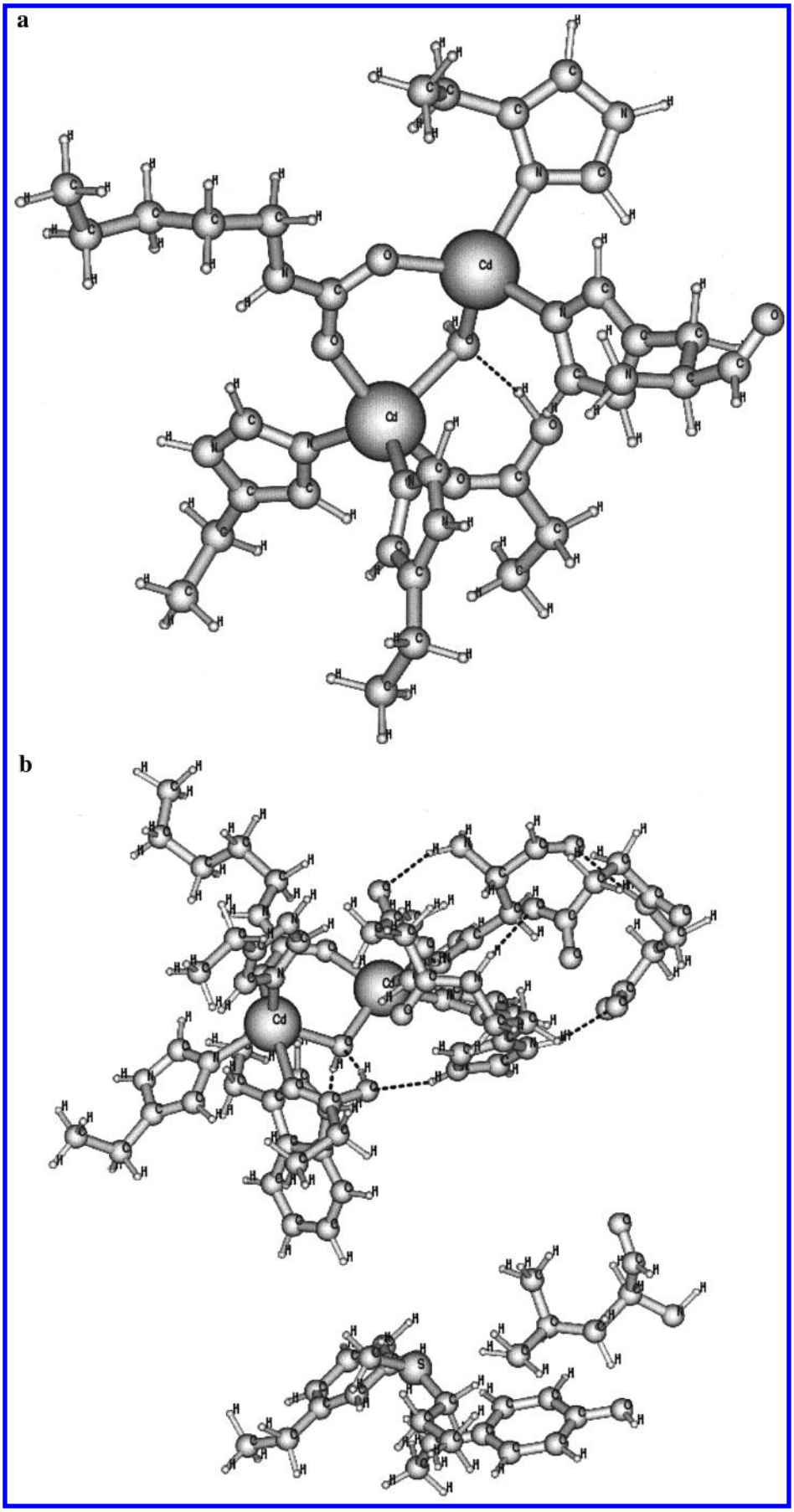

Figure 6. (a) Unconstrained structure of the protonated Cd−Cd active site: proton added to carboxylate, all-electron atoms. (b) Unconstrained structure of the protonated Cd−Cd active site: proton added to carboxylate, all-electron atoms, and EFP atoms.

represented as imidazole while the subsequent EFP optimizations require that the residues are modeled with all atoms to the C_α. The qualitative behavior of the proton binding does not change between the small inherent models and the EFP model including a full second shell of protein residues.

Since the possibility of the proton binding to the hydroxyl and yielding a bridging water is suggested only by the Cd−Cd X-ray structure, we will discuss the two protonated structures calculated in an unconstrained optimization with the EFP protein environment. Protonating the hydroxyl effectively separates the Cd ions since the water lacks the electrostatic potential to bridge these cations. The water remains bonded to Cd2, while the carbamylated lysine carboxylate maintains a strained bond to Cd1 with a more normal bond to Cd2 as seen in Figure 5a. The water maintains the H-bond to the carboxylate of D301, retaining an ionic active site that is still able to activate a water nucleophile. The local environment around each Cd cation is now tetrahedral, but the second shell H-bonds have not changed from the unprotonated active site as seen in Figure 5b. This structure is calculated to be slightly lower in energy (∼5 kcal/mol) than the one where the proton resides on the carboxylate of D301. However, there is more movement in the C_α backbone for this case.

Binding the proton to D301 requires that the hydroxyl rotates to allow the D301 to be the proton donor. However, little changes in the H-bonds to the protein second shell with an H-bond from the H254 to D301. The bond distance from Cd1 to OD1 of D301 is now 2.46 Å, in closer agreement with the experimental value. The Cd−Cd distance is 3.88 Å, which is only slightly increased over the value for the unprotonated active site. Within the experimental errors it is difficult to choose for the Cd−Cd enzyme between these two model structures. The absence of bound water(s) or any inhibitor in the present model also increases the difficulty of making an assignment of the ionicity of the experimental structure. The present geometries alone will not allow us to discriminate, and we will have to add waters and consider spectroscopic properties, which are not yet available experimentally, to finally judge.

4. CONCLUSION

The combination of the use of the ECP and EFP make more realistic calculations of the structures possible of metal-substituted enzyme active sites with different ionicities. The ECP are required because of the presence of transition metals and the relatively large number of electrons. Even the removal of the K electrons from first-row atoms is significant as the number of basis functions gets large because of the N^3 scaling. If all the atoms considered as EFP were treated all-electron, the number of basis functions would exceed 1200. Optimization of a structure with over 200 atoms and this number of basis functions is presently impossible. The ECP were parametrized using Dirac−Fock wave functions, so heavier metals can be considered accurately. The EFP are chosen to represent the second shell in the Zn−Zn enzyme but are suitable for the optimization of other metal-substituted active sites as shown by the calculation of the Cd−Cd site in reasonable agreement with experiment. The siting of waters in the active site will require more analysis, but the experimental and theoretical evidence suggests strong interaction with the bridging ligands and the possibility of multiple binding positions. Protonation of the Cd−Cd enzyme is possible at more than one site with comparable energetics. Water formed from protonation of the hydroxyl ligand will not serve as a bridging ligand, and the Cd−Cd distance will exceed 5 Å. Protonation of the D301 carboxylate changes the active site geometry relatively slightly. Within the accuracy of both the experimental and theoretical distances, it is then difficult to choose whether the site is protonated or not. The pH at which the crystal was formed suggests the site is not protonated, but there is no definitive structural evidence. Electronic properties would be very different, and these can be calculated for the enzyme active site.

ACKNOWLEDGMENT

This work was supported in part by the Advanced Technology Program of the National Institute for Standards and Technology.

REFERENCES AND NOTES

(1) Jensen, J. H.; Day, P. N.; Gordon, M. S.; Basch, H.; Cohen, D.; Garmer, D. R.; Krauss, M.; Stevens, W. J. *Modeling the Hydrogen Bond*; Smith, D. A., Ed.; ACS Symposium Series 569; American Chemical Society: Washington, DC, pp 139−151.
(2) Day, P. N.; Jensen, J. H.; Gordon, M. S.; Webb, S. P.; Stevens, W. J.; Krauss, M.; Garmer, D.; Basch, H.; Cohen, D. *J. Chem. Phys.* **1996**, *105*, 1968.
(3) Stevens, W. J.; Basch, H.; Krauss, M. *J. Chem. Phys.* **1984**, *81*, 6026.
(4) Stevens, W. J.; Krauss, M.; Basch, H.; Jasien, P. G. *Can. J. Chem.* **1992**, *70*, 612.
(5) Tuovinen, K.; Korhonen, E. K.; Raushel, F. M.; Hanninen, O. *Fundam. Appl. Toxicol.* **1996**, *31*, 210.
(6) Vilanova, E.; Sogorb, M. A. *Crit. Rev. Toxicol.* **1999**, *29*, 21.
(7) Hong, S.; Raushel, F. M. *Biochemistry* **1996**, *35*, 10904.
(8) Watkins, L.M.; Kuo, J. M.; Chen-Goodspeed, M.; Raushel, F. M. *Proteins* **1997**, *29*, 553.
(9) Vanhooke, J. L.; Benning, M. M.; Raushel, F. M.; Holden, H. M. *Biochemistry* **1996**, *35*, 6020.
(10) Benning, M. M.; Kuo, J. M.; Raushel, F. M.; Holden, H. M. *Biochemistry* **1995**, *34*, 7973.
(11) Garmer, D. R.; Krauss, M. *J. Am. Chem. Soc.* **1993**, *115*, 10247.
(12) Argos, P.; Garavito, M.; Eventoff, W.; Rossman, M. G. *J. Mol. Biol.* **1978**, *126*, 141.
(13) Alberts, I. L.; Nadassy, K.; Wodak, S. *J. Protein Sci.* **1998**, *7*, 1700.
(14) Christianson, D. W. *Adv. Prot. Chem.* **1991**, *42*, 281.
(15) Ryde, U.; Olsson, M. H. M.; Pierloot, K.; Roos, B. O. *J. Mol. Biol.* **1996**, *261*, 586.
(16) Dekerpel, J. O. A.; Pierloot, K.; Roos, B. O. *J. Phys. Chem. B* **1998**, *102*, 4638−47.
(17) Pierloot, K.; DeKerpel, J. O. A.; Ryde, U.; Roos, B. *J. Am. Chem. Soc.* **1997**, *119*, 218−26.
(18) Pierloot, K.; DeKerpel, J. O. A.; Ryde, U.; Olsson, M. H. M.; Roos, B. O. *J. Am. Chem. Soc.* **1998**, *120*, 13156.
(19) De Kerpel, J. O. A.; Ryde, U. *Proteins* **1999**, *36*, 157.
(20) Kafafi, S.; Krauss, M. *Int. J. Quantum Chem.* **1999**, *75*, 289.
(21) Zhan, C.; de Souza, N. O.; Rittenhouse, R.; Ornstein, R. L. *J. Am. Chem. Soc.* **1999**, *121*, 7279.
(22) Gilson, H. S. R.; Krauss, M. *J. Am. Chem. Soc.* **1999**, *121*, 6984.
(23) Gilson, H. S. R.; Gresh, N.; Krauss, M. Ab initio inherent structures of the zinc-lactamase active site: Effect of water binding, protonation state, and protein environment. Manuscript in preparation.
(24) Wilcox, D. E. *Chem. Rev.* **1996**, *96*, 2435−58.
(25) Schmidt, M. W.; Baldridge, K.; Boatz, J. A.; Elbert, S. T.; Gordon, M. S.; Jensen, J. H.; Koseki, S.; Matsunaga, N.; Nguyen, K. A.; Su, S.; Windus, T. L.; Dupuis, M.; Montgomery, J. A. *J. Comput. Chem.* **1993**, *14*, 1347.
(26) Worthington, S. E.; Krauss, M. *Comput. Chem.* **2000**, in press.
(27) Dumas, D. P.; Raushel, F. M. *J. Biol. Chem.* **1990**, *265*, 21498.
(28) Omburo, G. A.; Kuo, J. M.; Mullins, L. S.; Raushel, F. M. *J. Biol. Chem.* **1992**, *267*, 13278.

CI000046B